Modeling, simulation, analytic linearization and optimal control of a 6 tendon-driven biomimetic eye: a tool for studying human oculomotor control

Bernardo das Chagas e Silva Colaço Dias
Instituto Superior Técnico
Lisboa,Portugal
bernardo.colaco.dias@tecnico.ulisboa.pt

***Abstract*—The brain is a pivotal organ in animal systems. However, it is not yet fully understood how it controls all the other subsystems that compose the full organism. One of these subsystems, the oculomotor system, will be the main focus of this work. It is our objective to study the properties of the eye movement when redirecting our line of sight. We expanded the existing simulator and optimal control strategies in order to mimic human saccades (rapid eye movements). However, in the real system muscles can only exert force in one direction, meaning they only pull the eye, never push. We can see this as some sort of rubber band: if it is not stretched, it goes slack. The previous developed system did not incorporate this limitation, and, therefore, here, we attempted to eliminate this phenomenon.**

Since we are dealing with a non-linear system, in order to apply control strategies, the model had to be linearized. This is not a trivial task given the complexity of the dynamical equations and eye-direction dependent force computation. Furthermore, the eye kinematics are known to be determined by two degrees of orientational freedom (Listings' Law). Given that it is controlled by six independent muscles, this constraint to two degrees of freedom makes it an interesting problem to investigate. Although many studies have modeled the oculomotor system, most of them only do it on one dimension, and often only study either the kinematics or dynamics. We also use the relation between peak velocity, duration and amplitude, known as *Main Sequence* as a metric for evaluating our system emulation of the human eye.

Furthermore, we worked towards having accurate results regarding the kinematics and dynamics of this system, considering all degrees of freedom. So, all aspects of shifting our gaze (eye orientation with respect to the world) will be analysed: eye orientations, velocity profiles, torsion and optimal motor commands.

***Index Terms*—Gaze, Listing's law, Saccadic movement, *Main Sequence*, Slack**

I. Introduction

For this work, our model was based on a more recently developed prototype (one with six independent motors), and, as such, we separated each individual muscle, giving the eye 3 extra degrees of freedom. Contrary to the model developed before, this new model is closer to the actual human eye anatomy, where muscles have different length, making it an asymmetrical model [1]. Another problem is that the eye muscles can not push, which means it can only exert force in one direction. This requires the muscles to be tense to move the eye. So we wish to eliminate the possibility of the muscles going slack (having a smaller length than the initial one). Additionally, in this work, the dynamics of the system can be linearized at any equilibrium point in the eye's visual range, allowing the control to be better suited for saccades not starting from the origin. Finally, we extended the dynamical analysis of our simulator to a coupled eye-head orienting system, which will allow future studies to also include combined eye-head movements in three dimensions.

Our main goals are to separately control all 6 extraocular muscles (EOM), similar to the actual system, model the head dynamics, linearize the system (so that we can have an approximation of the dynamics of the system at any equilibrium point), and implement a control strategy that provides accurate results even with the asymmetry of the extraocular muscles. The last objective of this work, is to eliminate slack of the muscles, in an attempt to be even closer to human behavior.

II. Background

A. Eye mechanical and dynamical properties

Donders' law states that, for any single direction, the eye will always have the same unique orientation in three dimensions. Let's consider this example: if the target is in a downward and left direction, the eyes' orientation will be the same no matter the path they take: whether they go down first and then left or left first and then down, or direct along some oblique or curved path. There are different explanations for the origin of this law: either it is imposed entirely by the ocular muscle mechanics, or it is the result of a neural strategy that aims to optimize certain perceptual and/or motor performance criteria [2].

Listing's law for the eye may be regarded as a specification of Donders' law. While Donders stated that the orientation of the eye for a specific gaze direction was fixed, Listing went one step further, by realizing that any orientation of a rigid body can be achieved by a hypothetical single-axis rotation from some fixed origin, so-called primary position.

Listing's law then states that the torsional component of the rotation axes for all eye orientations is zero.

The main sequence is a well-known relationship between duration, velocity and amplitude of head-fixed saccadic movements. It has been shown that for a given amplitude, there is an optimal eye trajectory, with an optimal duration and a generic velocity profile [3]. The duration of a saccade increases

linearly with amplitude, and with increasing amplitude the peak velocity increases as well, until it saturates.

B. State of the art

A recent study on physical modeling of the eye [4], developed a robotic prototype of the eye with three degrees of rotational freedom that obeys Listing's law. The authors were able to build a tendon driven prototype (but only with 4 tendons,) focusing on showing that the compliance with Listing's law can be achieved using particular geometry (functionally incorporating the EOM pulley system, in order to mechanically fix Listing's plane) and placement of four extraocular muscles. However, they did not study the dynamics nor the control. Also, it has been shown that the actual eye can move out of Listing's plane, so mechanically constraining it to follow Listing's law seems limiting, considering the objectives of this thesis.

An anatomically accurate model of the oculomotor system was described in [5]. This work was based on the work from the founder of this field, DA Robinson in 1975 [6]. From MRI scans, they were able to build 3D non-linear geometric models of the EOM and investigate how they influence eye movement. They studied different computational models of the muscles in order to generate correct eye kinematics, fitting it to experimental data without emphasis on understanding the underlying control or the Listing's law compliance.

III. Methods

In this work we build an eye-head simulator but will concentrate our efforts in the eye saccadic control. Thus, we create a biologically inspired model for eye kinematics, dynamics and actuator, considering possible robotics implementation. Furthermore, we design a simplified head model, to be further developed in future work. The eye was designed as a ball joint, subject to the Newton's rigid body equations, and Euler's equation of motion with six tendon-driven actuators mimicking the human eye muscle kinematics. We also define the system parameters of inertia, stiffness and damping to replicate closely the time constants and overdamped characteristics of the human eye.

A. Eye model

The model in this work is not the exact dimension of the human eye. Actually, our model is developed after a robotic prototype developed to study biomimetic eye movements. Our robot model is around three times bigger than a real eyeball. Furthermore, relative to the eye's inertia tensor, ours is around 1000 times higher than the approximate inertia tensor built to represent the human eye, calculated using its mass and dimensions. Also, the head inertia was scaled to match the eye's proportions. Although our artificial eye's parameters are different from the human eye, they are configured to roughly replicate its main dynamics characteristics in terms of time constants and damping. These are important features to develop controllers that can give us insights on human oculomotor control.

The eye and head are connected through six extraocular muscles. Thus, one point of each muscle is attached to the head and the other end to the eye (fig 1). The extraocular muscles are roughly arranged according to the anatomy of the human eye [1] (their geometric display is shown in figure 1). In reality, these muscles are not actually completely straight.

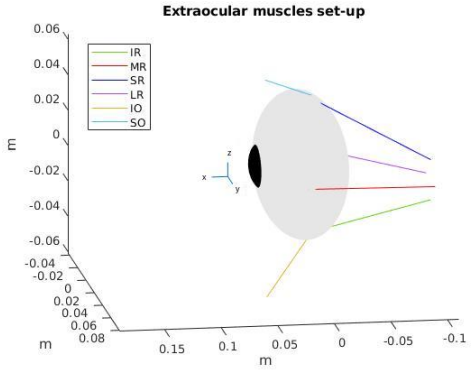

Fig. 1. Insertions points on the right eye and head of the extraocular muscles (left and rear view). The head is not shown, but it would encompass the eye and EOM. It has the same center of rotation as the eye.

It happens that in the human eye, the contact locus between the muscle and the eye is not really a point, but a curve. For now, we are simplifying this fact by considering it a mere point (the last point of contact). In the real system, the elastic component of the muscles make them go stiffer or relax by a certain amount, rotating the eye. Since it's very difficult to develop a prototype of a spring that changes stiffness, our robot artificial eye implements this by making the change in length of the muscle (making it exert a different amount of force), move the eye. In our model, the cables are wrapped around a spindle attached to a motor.

Eye dynamics can be described according to

$$ {}^{e}\boldsymbol{\alpha}_{h,e} = {}_{e}\mathbf{I}_{e}{}^{-1}({}_{e}\boldsymbol{\tau}_{eye} - {}^{e}\boldsymbol{\omega}_{h,e} \times {}_{e}\mathbf{I}_{e}\,{}^{e}\boldsymbol{\omega}_{h,e}) \tag{1} $$

In order to ease the understanding of the system, a real time graphical simulator was built to show the behavior of the numerical simulator. It can be seen in figure 2. This tool was done resorting to *ROS* graphical capabilities, namely *RVIZ*.

B. Head model

Since the focus of this work is the eye saccadic control, we simplify the head model as a sphere that rotates arbitrarily around the same point as the eye. This sphere is coupled in the neck through elastic springs and generalized friction. In order to rotate said sphere, generic torques can be directly applied. Head dynamics can be described by

$$ {}^{h}\boldsymbol{\alpha}_{w,h} = {}_{h}\mathbf{I}_{h}{}^{-1}({}_{h}\boldsymbol{\tau}_{head} - {}^{h}\boldsymbol{\omega}_{w,h} \times {}_{h}\mathbf{I}_{h}\,{}^{h}\boldsymbol{\omega}_{w,h}) \tag{2} $$

C. Linearization

In order to control the system, a linear approximation of the kinematics is convenient, since a highly non-linear system like the one modeled is not trivial to control. These non-linearities (e.g. force computation, rotation matrices) also proved hard to

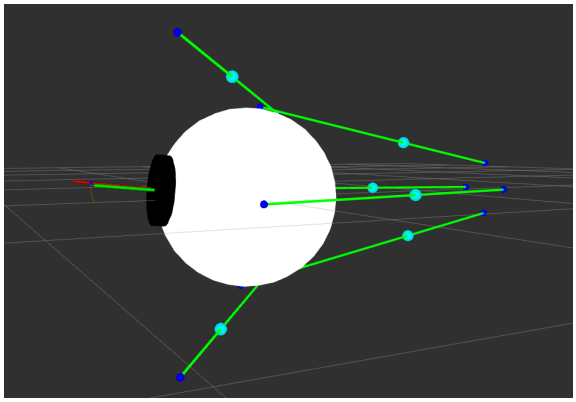

Fig. 2. Developed eye graphical simulator

differentiate, needing a fair amount of mathematical research and understanding. The linearization performed was based on an analytical perturbation, in which an infinitesimal perturbation was applied to the system around an equilibrium point to get a response from the linearized system that approximates the non-linear response [7]. In order to do this, first it is required to define a state-space model. The first step is to define the differential equations that represent the system's dynamics.

$$ {}^{w}\dot{\mathbf{R}}_e = {}^{w}\mathbf{R}_e \, {}^{e}\boldsymbol{\omega}^{\wedge}_{w,e} \tag{3} $$

$$ {}^{w}\dot{\mathbf{R}}_h = {}^{w}\mathbf{R}_h \, {}^{h}\boldsymbol{\omega}^{\wedge}_{w,h} \tag{4} $$

$$ {}^{e}\dot{\boldsymbol{\omega}}_{w,e} = {}_{e}I_e{}^{-1}({}_{e}\boldsymbol{\tau}_{eye} - {}^{e}\boldsymbol{\omega}_{w,e} \times {}_{e}I_e \, {}^{e}\boldsymbol{\omega}_{w,e}) \tag{5} $$

$$ {}^{h}\dot{\boldsymbol{\omega}}_{w,h} = {}_{h}I_h{}^{-1}({}_{h}\boldsymbol{\tau}_{head} - {}^{h}\boldsymbol{\omega}_{w,h} \times {}_{h}I_h \, {}^{h}\boldsymbol{\omega}_{w,h}) \tag{6} $$

we represent an equilibrium point by

$$ \bar{\mathbf{x}} = \left\{ {}^{w}\bar{\mathbf{R}}_e, {}^{w}\bar{\mathbf{R}}_h, {}^{e}\bar{\boldsymbol{\omega}}_{w,e}, {}^{h}\bar{\boldsymbol{\omega}}_{w,h} \right\} \tag{7} $$

which satisfies the condition

$$ f(\bar{\mathbf{x}}, \bar{\mathbf{u}}) = 0 \tag{8} $$

where $\bar{\mathbf{u}}$ is the input command that makes the dynamic equation be zero. According to equations (3-6) this happens when

$$ \begin{aligned} \boldsymbol{\tau}_{eye} &= 0 \\ \boldsymbol{\tau}_{head} &= 0 \\ {}^{e}\bar{\boldsymbol{\omega}}_{w,e} &= 0 \\ {}^{h}\bar{\boldsymbol{\omega}}_{w,h} &= 0 \end{aligned} $$

Let us define a local state around the equilibrium point $\bar{\mathbf{x}}$ as

$$ \tilde{\mathbf{x}} = \left\{ {}^{w}\tilde{\mathbf{R}}_e, {}^{w}\tilde{\mathbf{R}}_h, {}^{e}\tilde{\boldsymbol{\omega}}_{w,e}, {}^{h}\tilde{\boldsymbol{\omega}}_{w,h} \right\} \tag{9} $$

with

$$ {}^{w}\tilde{\mathbf{R}}_e = {}^{w}\bar{\mathbf{R}}_e^{T} {}^{w}\mathbf{R}_e \tag{10} $$

$$ {}^{w}\tilde{\mathbf{R}}_h = {}^{w}\bar{\mathbf{R}}_h^{T} {}^{w}\mathbf{R}_h \tag{11} $$

$$ {}^{e}\tilde{\boldsymbol{\omega}}_{w,e} = {}^{e}\boldsymbol{\omega}_{w,e} - {}^{e}\bar{\boldsymbol{\omega}}_{w,e} \tag{12} $$

$$ {}^{h}\tilde{\boldsymbol{\omega}}_{w,h} = {}^{h}\boldsymbol{\omega}_{w,h} - {}^{e}\bar{\boldsymbol{\omega}}_{w,h} \tag{13} $$

where $\tilde{\mathbf{R}}$ is the rotation between equilibrium orientation $\bar{\mathbf{R}}$ and the actual orientation $\mathbf{R}$. Using exponential notation, we can represent $\tilde{\mathbf{R}}$ with a rotational perturbation $\boldsymbol{\eta}$ as

$$ \tilde{\mathbf{R}}(t) = \exp(\boldsymbol{\eta}^{\wedge}) \tag{14} $$

At this point, let's consider the following simplification in the notation

$$ {}^{x}\boldsymbol{\omega}_{w,x} \equiv \boldsymbol{\omega}_x \tag{15} $$

$$ {}^{x}\tilde{\boldsymbol{\omega}}_{w,x} \equiv \delta\boldsymbol{\omega}_x \tag{16} $$

Adapted from [7], an infinitesimal variation, with respect to a reference $\bar{\mathbf{R}}(t) \in SO(3)$ is given by

$$ \delta\mathbf{R}(t) = \left. \frac{d}{d\epsilon} \right|_{\epsilon=0} \bar{\mathbf{R}}(t) \exp(\epsilon\boldsymbol{\eta}^{\wedge}) = \bar{\mathbf{R}}(t)\boldsymbol{\eta}^{\wedge}(t) \tag{17} $$

where ϵ is a small rotation around an axis .

From [8], the corresponding infinitesimal change in body angular velocities can be given as:

$$ \delta\boldsymbol{\omega}(t) = \boldsymbol{\omega}^{\wedge}(t)\boldsymbol{\eta}(t) + \dot{\boldsymbol{\eta}}(t) \tag{18} $$

Let's also consider the following exponential coordinates

$$ \boldsymbol{\eta}_e = \log({}^{w}\tilde{\mathbf{R}}_e)^{\vee} \tag{19} $$

$$ \boldsymbol{\eta}_h = \log({}^{w}\tilde{\mathbf{R}}_h)^{\vee} \tag{20} $$

These two equalities allow for elements of our local state to be mapped into the Lie group of the global state and vice-versa.

Our local state can thus, be represented in local coordinates, as :

$$ \xi = \begin{bmatrix} \boldsymbol{\eta_e} \\ \boldsymbol{\eta_h} \\ \delta\boldsymbol{\omega}_e \\ \delta\boldsymbol{\omega}_h \end{bmatrix} \tag{21} $$

This state is a vector in the tangent space, as represented in figure 3, of the Lie group $\mathcal{S}$ (containing our global state), considered at some point $x \in \mathcal{S}$, represented by

$$ T_x\mathcal{S} := \mathbb{R}^3 \times \mathbb{R}^3 \times \mathbb{R}^3 \times \mathbb{R}^3 \tag{22} $$

From (18), we can write our first two local state equations as:

$$ \dot{\boldsymbol{\eta}}_e = -\boldsymbol{\omega}_e^{\wedge}\boldsymbol{\eta}_e + \delta\boldsymbol{\omega}_e \tag{23} $$

$$ \dot{\boldsymbol{\eta}}_h = -\boldsymbol{\omega}_h^{\wedge}\boldsymbol{\eta}_h + \delta\boldsymbol{\omega}_h \tag{24} $$

and the complete equations (in matrix form) in the following way:

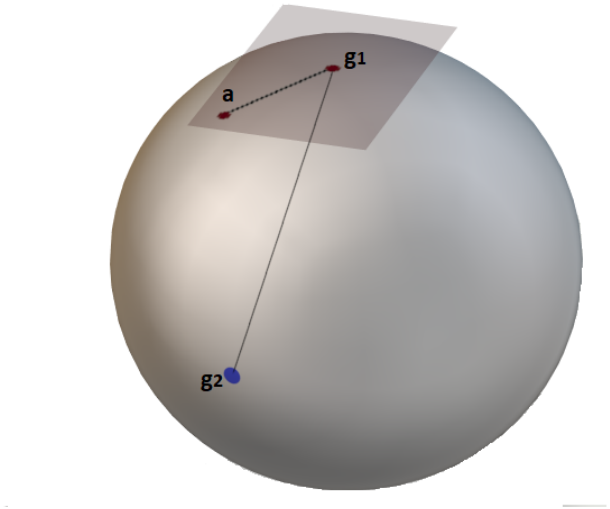

Fig. 3. Lie group transfer between the group and the tangent plane. Here, g_1 corresponds to $\bar{\mathbf{x}}$. a symbolizes $\boldsymbol{\xi}$ and can be mapped from the tangent space to the group, using exponential mapping, resulting in $g_2 = \mathbf{x}$ (7).

$$\dot{\boldsymbol{\xi}} = \frac{d}{dt}\begin{bmatrix} \boldsymbol{\eta}_e \\ \boldsymbol{\eta}_h \\ \delta\boldsymbol{\omega}_e \\ \delta\boldsymbol{\omega}_h \end{bmatrix} = \begin{bmatrix} -\boldsymbol{\omega}_e^{\wedge}\boldsymbol{\eta}_e + \delta\boldsymbol{\omega}_e \\ -\boldsymbol{\omega}_h^{\wedge}\boldsymbol{\eta}_h + \delta\boldsymbol{\omega}_h \\ {}_eI_e^{-1}\left({}_e\boldsymbol{\tau}_e - \boldsymbol{\omega}_e \times {}_eI_e\boldsymbol{\omega}_e\right) \\ {}_hI_h^{-1}\left({}_h\boldsymbol{\tau}_h - \boldsymbol{\omega}_h \times {}_hI_h\boldsymbol{\omega}_h\right) \end{bmatrix} \tag{25}$$

Knowing that in equilibrium, angular velocities are zero, we can show $\dot{\boldsymbol{\xi}}$ as a function of the local state $\boldsymbol{\xi}$ and command inputs $\mathbf{u}$.

$$\dot{\boldsymbol{\xi}} = f(\boldsymbol{\xi}, \mathbf{u}) \tag{26}$$

D. Jacobians

In order to have a linear state space model, a Jacobian linearization is performed. This is computed around an equilibrium point. The objective is to get a linear approximation of the non-linear state, which should be valid for small perturbations.

Dynamics of a general variation ($\delta_{\mathbf{x}}(t) = f(x, u)$) may be defined as

$$\dot{\delta}_{\mathbf{x}}(t) = f\left(\bar{\mathbf{x}} + \delta_{\mathbf{x}}(t), \bar{\mathbf{u}} + \delta_{\mathbf{u}}(t)\right) \tag{27}$$

Doing a Taylor's expansion on the right side, we have

$$\dot{\delta}_{\mathbf{x}}(t) \approx f(\bar{\mathbf{x}}, \bar{\mathbf{u}}) + \left.\frac{\partial f}{\partial \mathbf{x}}\right|_{\substack{\mathbf{x}=\bar{\mathbf{x}} \\ \mathbf{u}=\bar{\mathbf{u}}}} \delta_{\mathbf{x}}(t) + \left.\frac{\partial f}{\partial \mathbf{u}}\right|_{\substack{\mathbf{x}=\bar{\mathbf{x}} \\ \mathbf{u}=\bar{\mathbf{u}}}} \delta_{\mathbf{u}}(t) + \tag{28}$$

$$\epsilon\left(\left\|\delta_{\mathbf{x},\mathbf{u}}(t) - \delta_{\mathbf{x},\mathbf{u}}(t)\big|_{\substack{\mathbf{x}=\bar{\mathbf{x}} \\ \mathbf{u}=\bar{\mathbf{u}}}}\right\|^2\right) \tag{29}$$

If it is linearized around an equilibrium point ($f(\bar{\mathbf{x}}, \bar{\mathbf{u}}) = 0$), and neglecting higher order terms, we get

$$\dot{\delta}_{\mathbf{x}}(t) \approx \left.\frac{\partial f}{\partial \mathbf{x}}\right|_{\substack{\mathbf{x}=\bar{\mathbf{x}} \\ \mathbf{u}=\bar{\mathbf{u}}}} \delta_{\mathbf{x}}(t) + \left.\frac{\partial f}{\partial \mathbf{u}}\right|_{\substack{\mathbf{x}=\bar{\mathbf{x}} \\ \mathbf{u}=\bar{\mathbf{u}}}} \delta_{\mathbf{u}}(t) \tag{30}$$

Adapting (28) to our case where f depends on our local state $\boldsymbol{\xi}$ and input $\mathbf{u}$. The Taylor series around a fixed point $(\bar{\boldsymbol{\xi}}, \bar{\mathbf{u}})$, can be written as

$$f(\boldsymbol{\xi}, \mathbf{u}) = f(\bar{\boldsymbol{\xi}}, \bar{\mathbf{u}}) + \mathbf{J}(\bar{\boldsymbol{\xi}})(\boldsymbol{\xi} - \bar{\boldsymbol{\xi}}) + \mathbf{G}(\bar{\mathbf{u}})(\mathbf{u} - \bar{\mathbf{u}}) \tag{31}$$

where $\mathbf{J}(\bar{\boldsymbol{\xi}})$ and $\mathbf{G}(\bar{\mathbf{u}})$ are the Jacobian matrices and the higher order terms of the Taylor Series expansion are neglected. Since $\bar{\boldsymbol{\xi}}$ is our state evaluated at an equilibrium point and at equilibrium, our local state is zero ($\bar{\xi} = 0$), we can write

$$f(\boldsymbol{\xi}, \mathbf{u}) = \mathbf{J}(\bar{\boldsymbol{\xi}})\boldsymbol{\xi} + \mathbf{G}(\bar{\mathbf{u}})(\mathbf{u} - \bar{\mathbf{u}}) \tag{32}$$

Instead of explicitly computing the partial derivatives of f with respect to each component of $\boldsymbol{\xi}$ and $\mathbf{u}$, an alternate way to compute the Jacobian matrix is to write f in the form of (32) and identify the term where the unit power of $\boldsymbol{\xi}$ appears to the right of a multiplication with a matrix. This matrix, evaluated at the equilibrium point, is the desired Jacobian ($\mathbf{J}$). The same logic applies to $\mathbf{G}$, but with a term where the unit power of $\mathbf{u}$ appears on the right.

From (30) we get a state in the form of

$$\dot{\boldsymbol{\xi}} = \mathbf{A}\boldsymbol{\xi} + \mathbf{B}\delta\mathbf{u} \tag{33}$$

where $\boldsymbol{\xi}$ is the local state, $\delta\mathbf{u} = \mathbf{u} - \bar{\mathbf{u}}$, is the control signal increment with respect to the equilibrium value.

E. Optimal Control

We wish to develop a controller for the dynamical system, over a time interval, so that the system's behavior is optimal according to some constraints. These constraints are usually modeled through a cost function.

Cost functions are functions that depend on the state variables, and the input commands. Optimal control tries to minimize a cost function to get the ideal duration of the saccade and control inputs, and therefore, an optimal performance from the system. In order to attain said input for each saccade, we apply the optimal control to the linear system (local state).

Summarizing, we wish to

$$\begin{aligned} &\underset{\mathbf{u},p}{\text{minimize}} \;\; J(\mathbf{u}, p, goal) = \sum^{t} \lambda_t J_t(\mathbf{u}, p, goal) \\ &\textbf{subject to} \\ &\qquad \mathbf{x}_{i+1} = \mathbf{A}\mathbf{x}_i + \mathbf{B}\mathbf{u}_i \\ &\qquad \mathbf{y}_i = \mathbf{C}\mathbf{x}_i, \qquad i = 0, 1, ..., p \\ &\qquad \mathbf{u} \geq 0 \end{aligned}$$

where J_t represents each cost term and λ_t is the weight associated with each individual cost term. p is the optimal saccade time. For each p we compute the costs and decide on the optimal time that has the minimum total cost for a specific saccade.

It's convenient to discretize the system in order to apply the optimal control, resulting in the system in the form of

$$\boldsymbol{\xi}^{(k+1)} = \mathbf{A}\boldsymbol{\xi}^{(k)} + \mathbf{B}\delta\mathbf{u}^{(k)}, \qquad k = 0, ..., p \tag{34}$$

1) Accuracy Cost: The accuracy term seeks to penalize eye movements that deviate from the goal orientation. This makes the system strive to get as close to the objective as possible. Our cost is taken as

$$J_x = \lambda_x (y(p) - g)^2 \tag{35}$$

where λ_x specifies the relative cost for inaccuracies, $y(p)$ is the final position (at time p) of the eye and g is the goal position. The position of the eye is the first component of our global state,${}^w\mathbf{R}_e$.

2) Duration Cost: This cost term aims to toll the time it takes to perform a saccade. We know that duration increases almost linearly with goal amplitude. However, our cost term does not rely on amplitude explicitly, since we want that the underlying dynamics of the eye satisfy *Main Sequence* relationships without forcing them directly. Our duration cost is given by

$$J_p = \lambda_p (1 - \frac{1}{1 + \beta p}) \tag{36}$$

where λ_p is the relative weight of this cost term, β is the rate of discount parameter (temporal reward decay) and p is the saccade duration.

3) Energy cost: Here, we aim to toll the energy expenditure. Since we assume the energy to be proportional to the actuator's rotation (angular velocity), and the timesteps to be uniform, we can simplify this term as the difference between angular positions at each timestep. This can simply be written as the difference between consecutive $u^{(i)}$'s.

$$J_e(\boldsymbol{u}) = \lambda_e \|\Delta \boldsymbol{u}\|^2 \tag{37}$$

where J_e is the effort cost, λ_e is the weight of this cost term and $\Delta\mathbf{u}$ is the difference between the current vector of motor commands and the previous.

In matrix form, this can be written as

$$J_e(u) = \lambda_e \| \begin{bmatrix} u_0 \\ u_1 - u_0 \\ \vdots \\ u_p - u_{p-1} \end{bmatrix} \|^2 \tag{38}$$

4) Equilibrium Cost: This term is taken with the purpose of penalizing the change in state when the eye reaches the goal. With this cost it is possible to toll the change in orientation and velocity, when compared to the state reached by the optimal control. The function that translates this objective into a mathematical context is:

$$J_{eq} = \lambda_{eq} (\mathbf{x}(p) - \mathbf{x}(p+1))^2 \tag{39}$$

where λ_{eq} is the weight given to this cost, $x(p)$ is the final state and the other term symbolizes the subsequent states.

5) Last command cost: Equilibrium and accuracy cost terms are computed using the approximated linear model, so they don't stabilize at the actual required goal. In order to make sure that the system stabilizes at the goal orientation, we calculate a desired final input from equilibrium conditions and toll the deviation from that set of commands. Putting this in equation form, we get

$$J_{uacc} = \lambda_{uacc} (\mathbf{u}(p) - \mathbf{u}_{des})^2 \tag{40}$$

where λ_{uacc} is the relative weight of this cost, $\mathbf{u}(p)$ is the set of optimal commands at the final time step for a specific goal, given by the optimal control solver and $\mathbf{u}_{des}$ is the set of commands that ideally would lead to goal orientation given by the solution of the equilibrium equations (8). These ideal commands are gotten from a "lookup" table.

6) Total cost: The complete cost function is the sum of the previous functions

$$J = J_p + J_x + J_c + J_{eq} + J_{uacc} \tag{41}$$

F. Lookup Table

This approach consists of a search for equilibrium points around the oculomotor range. For each point obtained, the associated last commands that led the eye there were stored in a "lookup" table. A condition had to be satisfied in order for the equilibrium point to be stored: the final force for each muscle had to be higher than a given threshold in order not to have slack. So, after a random saccade goal is generated, we search the closest equilibrium point in the table and consider that the final ideal input is the one associated with that orientation in the table. More details on this approach are explained in section IV.

IV. Results

A. Step Responses

The calibration of the damping and stiffness parameters for the eye were iterated knowing that the system's slowest time constant is around 200 ms [9]. It is also known that the eye can be well represented by a second order overdamped system, which means the step response does not oscillate and has a somewhat slow stabilization process. Given these properties, the eye simulator is true to the real system, since it respects the above characteristics, as can be seen in figure 4.

Head inertia is modelled to be around 1000 times bigger than the eye's. The human head, without neural control is thought to be well approximated by an underdamped system [10]. This behavior can be seen in figure 5. The settling time is also around 10 times bigger than the eye's, even for small rotations. The head, like the eye, is modelled as an isotropic system, not privileging the dynamics in any direction. However, the neck has a higher stiffness in the torsional dimension, not allowing the head to rotate as much in this direction. The step response for the coupled system was also tested. In order to check this, two tests were made: make the head move and check the eye's passive motion, and make the eye move and check the head's resulting motion. Since the

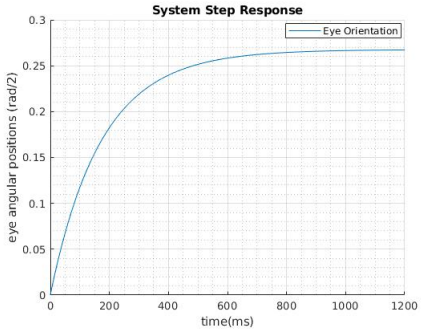

Fig. 4. Step response for the eye, when the inputs are motor controls that lead the system to perform a 30 degree purely horizontal rotation. In order to achieve this behavior damping and elasticity matrices are isotropic and have values of 0.04 Nms and 20 N, respectively. Regarding the inertia, $I_{xx} = 0.48$ $I_{yy} = 0.43$ $I_{zz} = 0.39$.

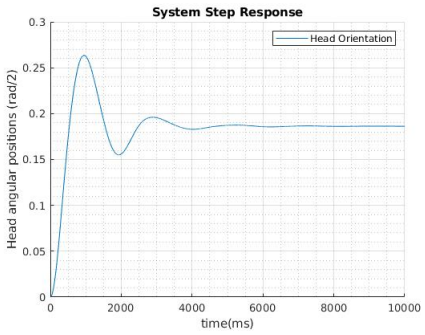

Fig. 5. Step response for the head, when the inputs are motor controls that lead the system to perform a saccade of 20 degrees purely horizontal rotation. The values for elasticity and damping matrices are 1 and 35, respectively. The inertia was $I_{xx} = 181$ $I_{yy} = 215$ $I_{zz} = 142$.

head is a lot heavier than the eye, it is expected that the eye's passive motion is largely motion by the head. On the other hand, it is expected that the eye's motion barely influences the head, given their inertia differences. The results can be seen in figures 6 and 7.

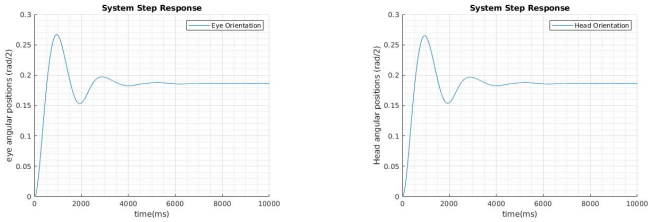

Fig. 6. It can be seen that an input on the head to make it move, drags the eye with it, i.e., the eye passively has the exact same behavior as the head, with a few milliseconds of delay.

As expected it was observed that the eye's passive movement when the head rotates is quite accentuated, but the head's motion when the eye rotates is negligible.

B. Lookup Table

This approach was thought to be a biologically plausible strategy, and it consists on learning combinations of muscle

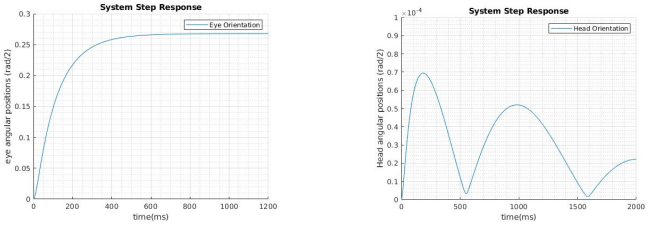

Fig. 7. When an input is applied only to the eye in order to check the head's passive movement, it can be seen that while the eye move's with it's usual overdamped behavior, the head is almost still (it actually moves around 0.0007 degrees, which is very small compared to the eye movement).

extensions associated with specific eye orientations.

1) Equilibrium Points: In order to gather equilibrium points, random step input combinations were given to the all motors in a range of $\pm$ 85 degrees, with the aim to find equilibrium orientations all around the eye's oculomotor range. If the combination of commands provided resulted in a stable equilibrium orientation, that set of inputs and resulting rotation vector was saved.

Figure 8 shows the distribution of the points stored in three dimensions. A skewness in equilibrium points can be observed, having less points on the right side of the plot. This is due to the asymmetry of the extraocular muscles, mainly between the horizontal pair.

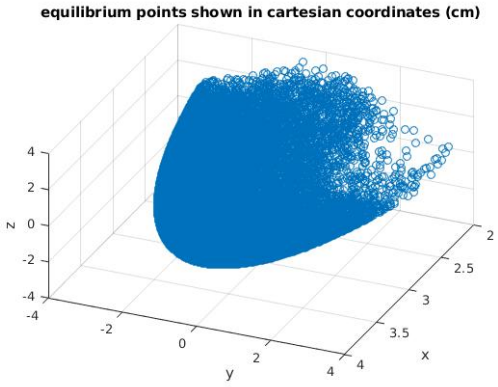

Fig. 8. Equilibrium points in the eye's visual range. There is a skewness in their distribution due to the asymmetry of the horizontal muscles. Around 20000 points were obtained and are shown here.

C. Listing's plane

250 random saccades were generated (with amplitudes from 5 to 40 degrees), using the optimal controller and their obedience to Listing's plane was evaluated, along with the verification of slack. The results from this experiment can be seen in figure 9. As it is noticeable, the biggest difference between the results from the previous approach is the mitigation of slack. Pre-tension had an important role in this task, by not letting the negative commands make the cables relaxed. Additionally, by identifying equilibrium orientations and storing them it was possible for the system to reach the goal orientation with

almost zero velocity. The major limitation that arises from this approach is the possibility of having a relevant accuracy error, since the goals are generated randomly and that specific orientation might not be an equilibrium position. However, from the tests performed it was observed that the error was almost always lower than 5 degrees. However, the maximum error was 7 degrees because the saccade goals implied a rotation to the right side, where we have fewer equilibrium points (figure 8). This is not optimal, but it is a trade-off so that it would be possible to eliminate slack. The standard deviation from Listing's plane was 1.17 degrees. For primates, studies have shown that this values is around 0.6 to 1.2 degrees. Even though our result is closer to the maximum value, proves the model and this approach are valid, and quite accurate.

The trajectories for these saccades can also be observed, to analyse if they also obey Listing's law. They can be seen in figure 10. During the trajectories there was no slack, and during the eye's movement until the goal, all orientations were in Listing's plane, and all trajectories were mainly straight, having low to null curvature. This shows that the controller makes the eye move in the optimal way, i.e., through the shortest path to the goal.

D. Main Sequence

As it can be observed in figure 11, the expected *Main Sequence* relations apply. Duration increases almost linearly with saccade amplitude due to the trade-off between duration and energy. The values of duration are also in agreement with neurological studies, having a value of around 200 ms for large saccades. Regarding the relation between peak velocity and amplitude, if one inspects the right plot from this figure, it is possible to notice that there is a linear increase on maximum angular velocity until around 400 deg/s. However, after this value, peak velocity saturates since the optimal controller does not allow the eye to reach greater speeds.

Another metric used to evaluate the functioning of this system is the skewness of saccades. In humans, peak velocity saturates at some point, but bigger saccades take longer to be executed. Furthermore, the acceleration velocity is similar for all amplitudes, which means that the difference of duration is due to the deceleration phase. This is the skewness of saccades. So, higher amplitude saccades have the same peak velocity, but take longer to reach equilibrium. The controlled simulator respects this behavior, as seen in figure 12. Leftward horizontal saccades with increasing amplitude were performed in order to test the skewness of saccades.

E. Muscle Responses

In the actual system, it has been shown that the neural signals that make the eye perform saccades are a combination between a pulse and a step signal. This means the muscle force should have a similar behavior. The results of this test can be observed in figure 13.

The initial forces are due to the pre-tension applied to the system so that the saccades would not have slack. The saccades performed for this test were negative horizontal rotations,

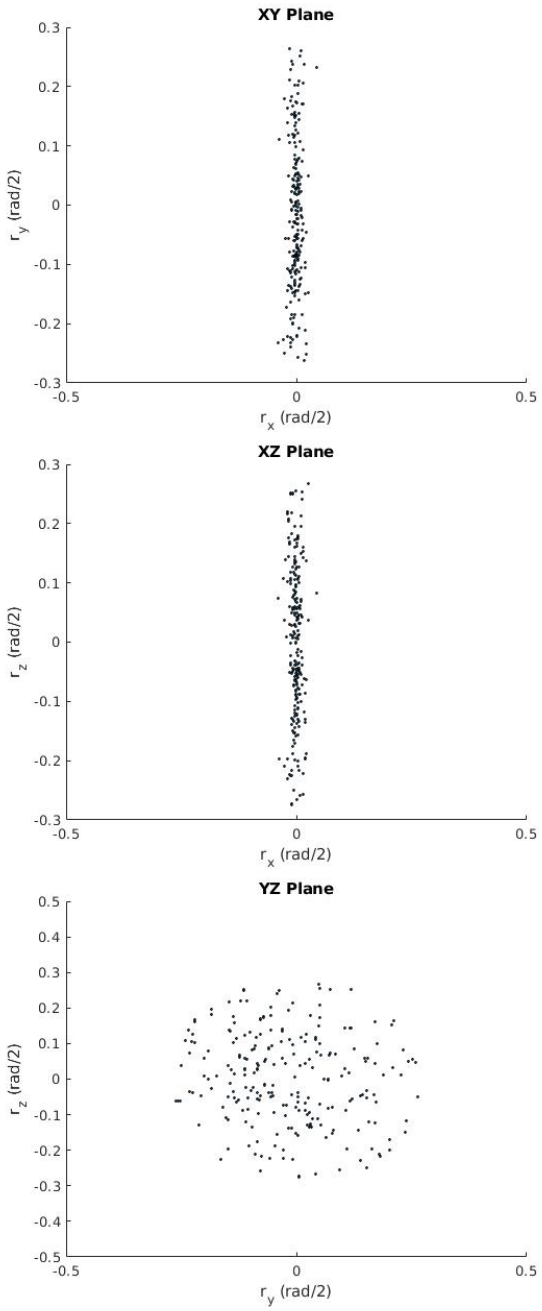

Fig. 9. 250 saccades' final eye orientations shown in 3 different planes. The standard deviation was of 1.17 degrees.

which make the Medial Rectus act as the antagonist and the Lateral Rectus act as the agonist. It is obvious that since the right graphic is for a bigger saccade, it takes more time to stabilize, and its force has a bigger magnitude. Regarding the shape of the muscle response, it can be seen that there is a pulse form, followed by a step shape. This is in accordance to what is thought to be the shape of the neural input signals.

It's interesting to see that during the saccade, the antagonist muscle (MR) relaxes, exerting less force, but during the fixation time, it actually has to apply more force on the eye

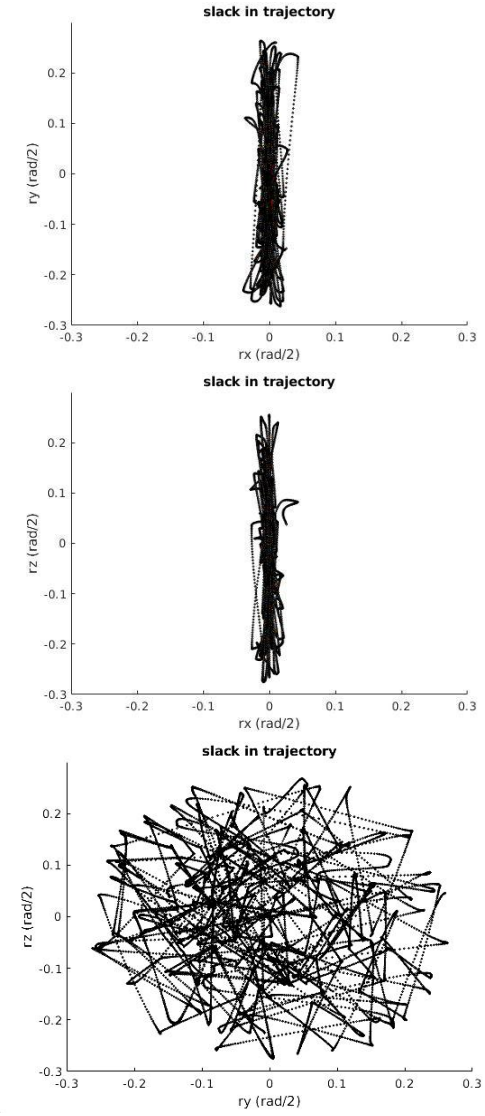

Fig. 10. Trajectories of the eye to reach the final orientations seen in figure 9. Maximum deviation from Listing's plane is 4.9 degrees.

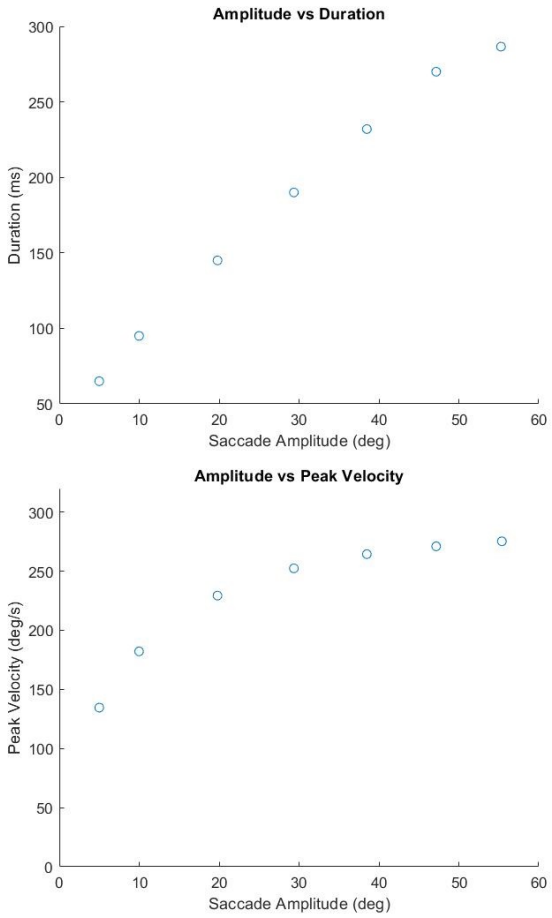

Fig. 11. Main Sequence behavior tested on the controlled simulator.

so that it fixates on the target (rightwards orientation).

V. Conclusions

One of the objectives of this work was to study the conditions that led the system to have slack. In order to do this several approaches were analysed. The one that mitigated this phenomenon was a memory-based approach, which might be a biologically valid approach, since it is reasonable to assume that it is easier for the brain to learn from experience an inverse kinematic map of the eye, than solving a non-linear system of equations at every single eye movement. The storage of optimal commands that lead to a specific eye orientation is a more realistic assumption.

The approaches tested resulted in a thin Listing's plane. However, slack tended to thicken said plane. Therefore, by erasing slack, we were able to reduce Listing's plane thickness, making the model more biomimetic. The non-linear properties

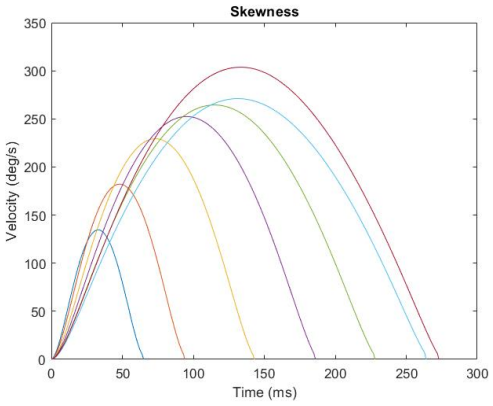

Fig. 12. Skewness of velocity profiles of saccades with increasing amplitudes. The rotations were all horizontal, starting from straight ahead orientation, and their magnitudes were, respectively 5, 10, 20, 30, 40, 50 and 55 degrees.

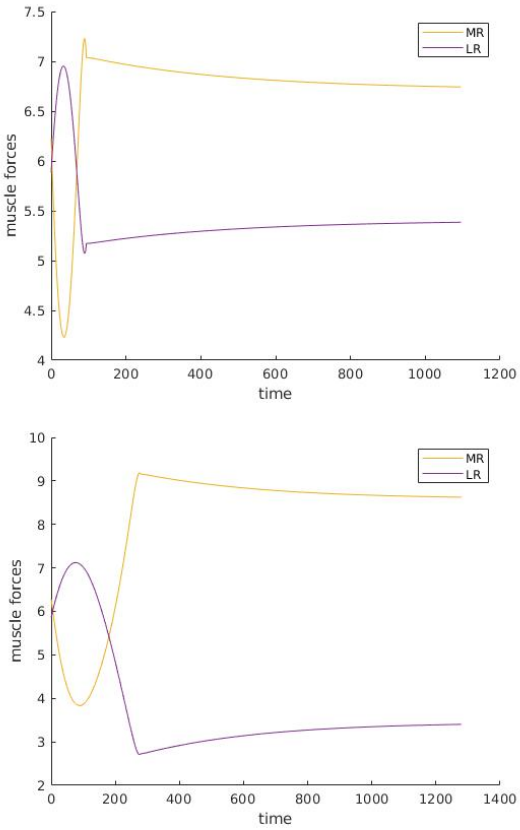

Fig. 13. Medial and Lateral rectus response in N to the commands that lead to rightwards horizontal saccades of 10 degres (left) and 55 degrees (right). Time axis is in ms.

that the human eye follows were also obtained using this approach, mainly due to the minimization of the energy and duration for each saccade.

REFERENCES

[1] J. M. Miller and D. A. Robinson, "A model of the mechanics of binocular alignment," *Computers and Biomedical Research*, vol. 17, no. 5, pp. 436–470, 1984.

[2] D. Tweed and T. Vilis, "Implications of rotational kinematics for the oculomotor system in three dimensions," *Journal of Neurophysiology*, vol. 58, no. 4, pp. 832–849, 1987.

[3] C. M. Harris and D. M. Wolpert, "The main sequence of saccades optimizes speed-accuracy trade-off," *Biological cybernetics*, vol. 95, no. 1, pp. 21–29, 2006.

[4] D. Biamino, G. Cannata, M. Maggiali, and A. Piazza, "Mac-eye: A tendon driven fully embedded robot eye," in *5th IEEE-RAS International Conference on Humanoid Robots, 2005.* IEEE, 2005, pp. 62–67.

[5] Q. Wei, *Biomechanical modeling and simulation of human eye movement*. Citeseer, 2010.

[6] D. A. Robinson, "A quantitative analysis of extraocular muscle cooperation and squint." *Investigative Ophthalmology & Visual Science*, vol. 14, no. 11, pp. 801–825, 1975.

[7] G. Wu and K. Sreenath, "Variation-based linearization of nonlinear systems evolving on $so(3)$ and s^2, 2015." *IEEE Access*, vol. 3, pp. 1592–1604, 2015.

[8] Y. Yu and X. Ding, "Trajectory linearization control on so(3) with application to aerial manipulation," *Journal of the Franklin Institute*, vol. 355, no. 15, pp. 7072 – 7097, 2018. [Online]. Available: http://www.sciencedirect.com/science/article/pii/S0016003218305222

[9] J. Van Opstal, *The auditory system and human sound-localization behavior*. Academic Press, 2016.

[10] G. Peng, T. Hain, and B. Peterson, "A dynamical model for reflex activated head movements in the horizontal plane," *Biological cybernetics*, vol. 75, no. 4, pp. 309–319, 1996.